Th SRS1 16

Anisotropic Elastic Wavefield Imaging Using the Energy Norm

D. Rocha* (Colorado School of Mines), N. Tanushev (Z-Terra Inc) & P. Sava (Colorado School of Mines)

SUMMARY

Based on the energy conservation principle, we derive a scalar imaging condition for anisotropic elastic wavefield migration. Compared to conventional imaging conditions that simply correlate displacement components or potentials from source and receiver wavefields, the proposed imaging condition does not suffer from polarity reversal, which might degrade the image quality after stacking over shots. Our imaging condition also accounts for the directionality of the wavefields in space and time, leading to attenuation of backscattering artifacts, which commonly appear in elastic reverse-time migration images with strong model contrasts. In addition, our new imaging condition does not require wave-mode decomposition, which demands significant additional cost for anisotropic wavefields. This new imaging condition relies on knowledge of the anisotropic model parameters used during migration, and is applicable for any kind of anisotropy. We show the quality of the energy image compared to its conventional counterparts by numerical experiments that simulate complex geological settings.

Introduction

A typical assumption in seismic wavefield imaging is that the subsurface is acoustic and isotropic. However, larger offsets and the increasing number of acquired azimuths require that we account for the influence of anisotropy; at the same time, the search for subsurface information such as fracture distribution encourages multicomponent elastic imaging. Although this technique has progressed greatly in recent years, a robust and effective method for elastic anisotropic imaging remains an elusive goal.

Wavefield imaging is implemented in two steps: wavefield extrapolation in the subsurface, using recorded data and an Earth model, and the application of an imaging condition to extract the Earth's reflectivity from the extrapolated wavefields (Claerbout, 1971). If a two-way elastic wave equation is used in the wavefield extrapolation, followed by the zero-lag crosscorrelation of the wavefields as the imaging condition, the procedure is called elastic reverse time migration (ERTM) (Chang and McMechan, 1987; Hokstad et al., 1998). Correlating the displacement fields for each component of the source and receiver wavefields is the most common imaging condition for elastic wavefields, generating images with a mixture of wave modes. Wave-mode decomposition for anisotropic wavefields is possible, but requires additional computational cost and robust techniques (Yan and Sava, 2009, 2011; Cheng and Fomel, 2013). In addition, polarity reversal occurs if one correlates different components of the displacement fields, and damages image quality after stacking over experiments (Balch and Erdermir, 1994). Similarly to wave-mode decomposition, polarity reversal corrections can be implemented with techniques that require additional cost for imaging (Duan and Sava, 2014). Moreover, backscattering artifacts occur if the migration velocity contains sharp contrasts, thus contaminating the image with low-wavenumber content (Yan and Xie, 2012). Ideally, these artifacts should be attenuated during imaging, without the use of post-imaging artificial filters such as the Laplacian operator (Zhang and Sun, 2009).

By defining an imaging condition that yields an attribute of the Earth's reflectivity into a single image without wave-mode decomposition, polarity reversal and backscattering artifacts, we seek to facilitate interpretation and provide a concise description of the subsurface structures. Our proposed imaging condition is formulated using the energy conservation principle, and extends previous work on isotropic elastic imaging (Rocha et al., 2015b).

Theory

For a general anisotropic medium, we can write the wave equation:

$$\rho\ddot{\mathbf{U}} = \nabla\cdot\left[\underline{\underline{\mathbf{c}}}\nabla\mathbf{U}\right] , \tag{1}$$

where $\mathbf{U}(\mathbf{x},t)$ is the elastic wavefield, $\underline{\underline{\mathbf{c}}}(\mathbf{x})$ is the fourth-rank stiffness tensor, and $\rho(\mathbf{x})$ is the medium density. The double dot indicates second derivative in time. Analogously to the acoustic and isotropic elastic cases discussed in Rocha et al. (2015a,b), we develop the energy function

$$E(t) = \frac{1}{2}\int_{\Omega}\rho\|\dot{\mathbf{U}}\|^2 + \left(\underline{\underline{\mathbf{c}}}\nabla\mathbf{U}\right) : \nabla\mathbf{U}\, d\mathbf{x} , \tag{2}$$

where Ω is the physical domain that contains the wavefield, and the symbol : indicates the element-wise inner product between matrices called Frobenius product. Equation 2 measures the total energy of the wavefield within a domain. Each one of the terms in equation 2 incorporates a particular physical meaning. The first term represents the kinetic energy of the wavefield, and the second term is the strain energy (Slawinski, 2003), which represents the potential energy of the wavefield.

Based on the energy conservation expression in equation 2, we can define a norm, and then, an inner product of two arbitrary elastic wavefields $\mathbf{U}$ and $\mathbf{V}$:

$$<\mathbf{U},\mathbf{V}>_E = \int_0^T\int_{\Omega}\rho\dot{\mathbf{U}}\cdot\dot{\mathbf{V}} + \left(\underline{\underline{\mathbf{c}}}\nabla\mathbf{U}\right) : \nabla\mathbf{V}\, d\mathbf{x} , \tag{3}$$

and an elastic imaging condition:

$$I_E = \sum_{e,t} \left[\rho \dot{\mathbf{U}} \cdot \dot{\mathbf{V}} + \left(\underline{\underline{\mathbf{c}}} \nabla \mathbf{U} \right) : \nabla \mathbf{V} \right] . \tag{4}$$

Here, e is the experiment index, which is commonly a shot record, $\mathbf{U}(e,\mathbf{x},t)$ and $\mathbf{V}(e,\mathbf{x},t)$ are the source and receiver displacement fields, respectively, and $I_E(\mathbf{x})$ is a scalar image obtained from the wavefields. We can also define the following multidimensional vector

$$\square \mathbf{U} = \left\{ \rho^{1/2} \dot{\mathbf{U}}, \underline{\underline{\mathbf{c}}}^{1/2} (\nabla \mathbf{U}) \right\} . \tag{5}$$

The vector in equation 5 contain twelve components, of which three components are from the particle velocity, $\dot{\mathbf{U}}$, and nine are from the displacement gradient, $\nabla \mathbf{U}$. A similar multidimensional vector can be defined for the receiver wavefield $\mathbf{V}$; therefore, we can rewrite equation 4 as the dot product between these vectors:

$$I_E = \sum_{e,t} \square \mathbf{U} \cdot \square \mathbf{V} . \tag{6}$$

This expression indicates that the energy elastic image is represented by the projection of the two multidimensional vectors onto one-another. Therefore, an image is formed when these space-time vectors are not orthogonal.

Vectors $\square \mathbf{U}$ and $\square \mathbf{V}$ are related to the polarization and propagation directions of the elastic wavefields $\mathbf{U}$ and $\mathbf{V}$. We can represent an elastic wavefield by

$$\mathbf{U} = \mathbf{u}_0 e^{i\omega(\mathbf{p}\cdot\mathbf{x} - t)} , \tag{7}$$

where $\mathbf{u}_0$ is the polarization vector, $\mathbf{p}$ is the slowness vector indicating propagation direction, and ω is the frequency. We assume that ω is large and that the vectors $\mathbf{u}_0$ and $\mathbf{p}$ are slowly varying in space and time, which makes their spatial and temporal derivatives small compared to ω. Equation 7 can be rewritten in index form as $U_i = u_i e^{i\omega(p_j x_j - t)}$, where index $i = \{1,2,3\}$ represents the Cartesian components of wavefield $\mathbf{U}$. Substituting the plane wave definition in equation 7 as trial solution of the elastic equation in 1, we obtain the Christoffel equation:

$$\rho u_i = u_k c_{ijkl} p_j p_l , \tag{8}$$

where $i,j,k,l = \{1,2,3\}$. We seek an imaging condition that attenuates waves of the source and receiver wavefields propagating along the same path and with the same polarization, i.e., elastic backscattering. Therefore, the backscattering events are characterized by $V_i = U_i = u_i e^{i\omega(p_j x_j - t)}$. Defining $(\square \mathbf{V})^\dagger$ with negative sign on the component containing the time derivative:

$$(\square \mathbf{V})^\dagger = \left\{ -\rho^{1/2} \dot{\mathbf{V}}, \underline{\underline{\mathbf{c}}}^{1/2} (\nabla \mathbf{V}) \right\} , \tag{9}$$

we can compute the dot product between $\square \mathbf{U}$ and $(\square \mathbf{V})^\dagger$ for backscattering events as

$$\square \mathbf{U} \cdot (\square \mathbf{V})^\dagger = \omega^2 \left[\rho u_i u_i - u_i u_k c_{ijkl} p_j p_l \right] e^{2i\omega(p_j x_j - t)} . \tag{10}$$

Using the relation in equation 8, we obtain

$$\square \mathbf{U} \cdot (\square \mathbf{V})^\dagger = 0 , \tag{11}$$

which means the dot product is zero everywhere except at locations where $\mathbf{p}$ and $\mathbf{u}_0$ are different for $\mathbf{U}$ and $\mathbf{V}$, i.e., at reflectors. Therefore, the dot product in equation 11 nullifies the events that propagate on the same path and have the same polarization. Such events include reflection backscattering, diving, direct and head waves from the same wave modes. Therefore, the imaging condition

$$I_E^\dagger = \sum_{e,t} \square \mathbf{U} \cdot (\square \mathbf{V})^\dagger \tag{12}$$

attenuates backscattering artifacts in anisotropic elastic RTM images, while retaining similar properties of the isotropic images discussed in Rocha et al. (2015b).

Example

Figure 1 shows the Marmousi-II (Martin et al., 2002) model parameters used to simulate synthetic data, the migration model parameters and the resulted images. The synthetic data are obtained from a horizontal line of receivers that record the displacement field at every grid point of the water bottom ($z = 0.5$ km), and from 76 pressure sources located near the surface of the water layer ($z = 0.05$ km) with a horizontal spacing of 150 m. This acquisition geometry resembles an ocean bottom seismic survey (OBS), recording multicomponent data at the water bottom. The migration model parameters are slightly smoothed versions of the true model parameters. As expected, all images contain backscattering artifacts, and Figure 1(h) also shows the effects of a non-constructive stack due to polarity reversal artifacts. In contrast, we attenuate all these artifacts in Figure 1(j) using the imaging condition from equation 12.

Conclusions

The energy imaging condition produces a scalar image without the need for wave-mode decomposition and does not suffer from polarity reversal, as is the case for displacement images using different components of the source and receiver wavefields. The proposed imaging condition incorporates propagation and polarization directions in its application, as inferred from the definition of the multidimensional vectors $\Box\mathbf{U}$ and $\Box\mathbf{V}$ built using the extrapolated wavefields $\mathbf{U}$ and $\mathbf{V}$. By properly applying a dot product between these multidimensional vectors, we are able to attenuate the backscattering artifacts in the imaging process, and obtain robust, cheap and high-quality elastic images.

Acknowledgements

We thank the sponsor companies of the Center for Wave Phenomena, whose support made this research possible. The reproducible numeric examples in this paper use the Madagascar open-source software package, freely available at http://www.ahay.org.

References

Balch, A.H. and Erdermir, C. [1994] Sign-change correction for prestack migration of P-S converted wave reflections. *Geophysical Prospecting*, **42**, 637-663.
Chang, W.F. and McMechan, G.A. [1987] Elastic reverse-time migration. *Geophysics*, **52**(10), 1365-1375.
Cheng, J. and Fomel, S. [2013] Fast algorithms for elastic-wave-mode separation and vector decomposition using low-rank approximation for anisotropic media. In: *SEG Houston 2013 Annual Meeting.*
Claerbout, J.F. [1971] Toward a unified theory of reflector mapping. *Geophysics*, **36**(3), 467-481.
Duan, Y. and Sava, P. [2014] Converted-waves imaging condition for elastic reverse-time migration. In: *SEG 2014 Denver Annual Meeting*.
Hokstad, K., Mittet, R. and Landrø, M. [1998] Elastic reverse time migration of marine walkaway vertical seismic profiling data. *Geophysics*, **63**(5), 1685-1695.
Martin, G., Marfurt, K. and Larsen, S. [2002] Marmousi-2, an updated model for the investigation of AVO in structurally complex areas. In: *2002 SEG Annual Meeting*.
Rocha, D., Tanushev, N. and Sava, P. [2015a] Acoustic wavefield imaging using the energy norm. In: *SEG New Orleans 2015 Annual Meeting*.
Rocha, D., Tanushev, N. and Sava, P. [2015b] Elastic wavefield imaging using the energy norm. In: *SEG New Orleans 2015 Annual Meeting*.
Slawinski, M.A. [2003] *Seismic Waves and Rays in Elastic Media*, 34. Elsevier Science, 1 edn.
Yan, J. and Sava, P. [2009] Elastic wave-mode separation for VTI media. *Geophysics*, **74**(5), WB19-WB32. Yan, J. and Sava, P. [2011] Elastic wave-mode separation for tilted transverse isotropy media. *Geophysical Prospecting*, **60**, 29-48.
Yan, R. and Xie, X.B. [2012] An angle-domain imaging condition for elastic reverse time migration and its application to angle gather extraction. *Geophysics*, **77**(5), S105-S115.
Zhang, Y. and Sun, J. [2009] Practical issues in reverse time migration: true amplitude gathers, noise removal and harmonic source encoding. *First Break*, **27**(1), 53-59.

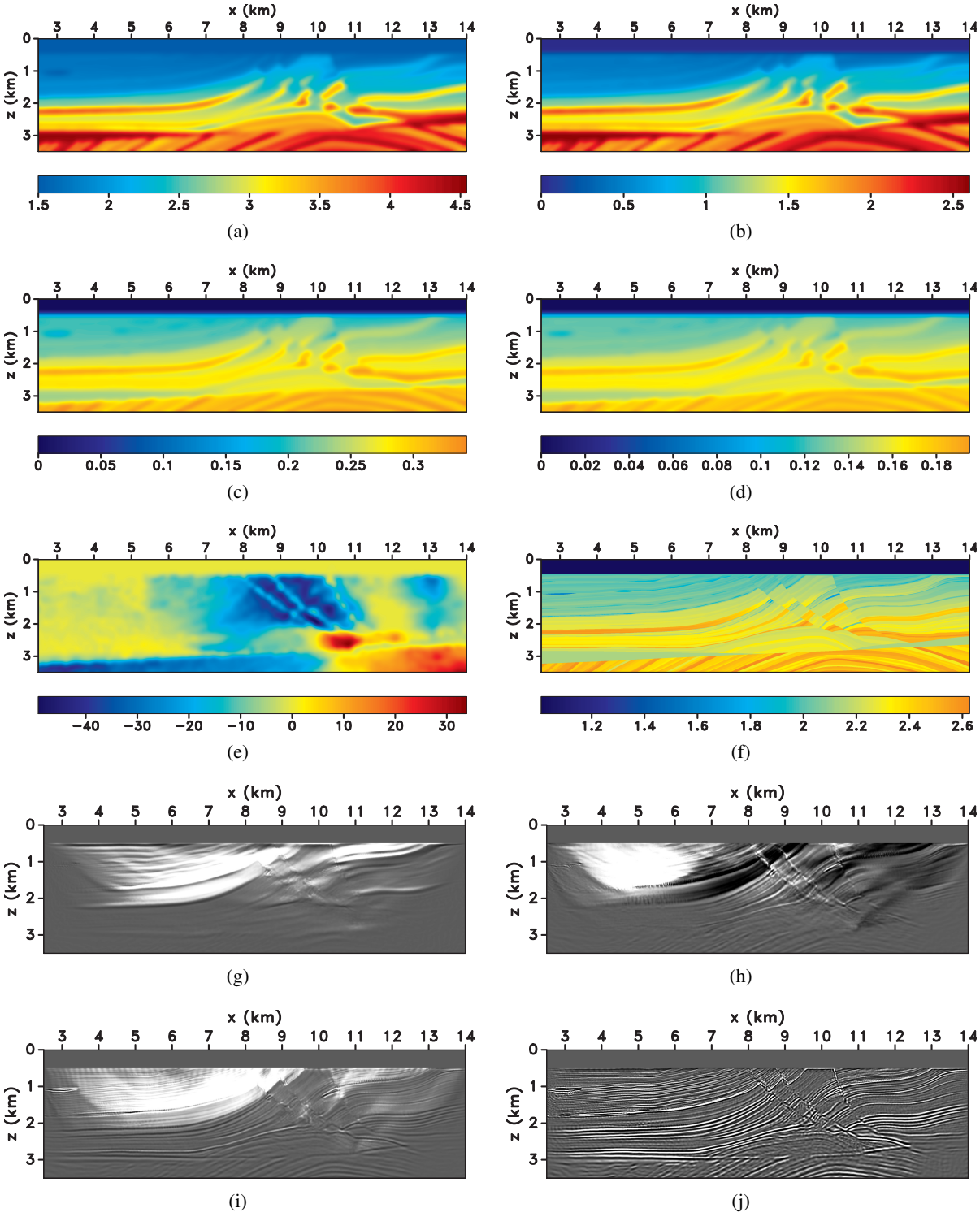


Figure 1 *Migration model parameters used for the Marmousi-II experiment. (a) P- and (b) S-wave velocity along the local symmetry axis (V_{P0} and V_{S0}, in km/s), (c) ε, (d) δ, (e) local tilt angle ν (in degrees). (f) Stratigraphic density model used to generate synthetic data (in g/cm^3). Images obtained using the correlation between displacement components (g) U_xV_x, (h) U_xV_z, and (i) U_zV_z; (j) energy image using the energy imaging condition in equation 12. The energy image shows strong reflectors undisturbed by either polarity reversal or backscattering events, with no additional post-imaging processing.*